2014

Fiber-Optic Temperature Sensor Using a Fabry–Pérot Cavity Filled With Gas of Variable Pressure

Yujie Lu
University of Nebraska-Lincoln, yujielu1219@gmail.com

Ming Han
University of Nebraska-Lincoln, mhan@egr.msu.edu

Jiajun Tian
University of Nebraska-Lincoln, jiajuntian@gmail.com

Pages: 757 - 760, DOI: 10.1109/LPT.2014.2304297

Fiber-Optic Temperature Sensor Using a Fabry–Pérot Cavity Filled With Gas of Variable Pressure

Yujie Lu, Ming Han, *Member, IEEE*, and Jiajun Tian

***Abstract*— We report a high-temperature fiber-optic sensor based on measuring the spectral fringes of a Fabry–Pérot (FP) cavity on a microstructure fiber (MF) when the gas pressure in the cavity is varied through the holes in the MF. Theoretical analysis shows that the absolute temperature can be deduced from the slope of the spectral shift versus pressure curve, which requires no calibration and is insensitive to the FP cavity length variations. For demonstration, we fabricated a miniature sensor whose FP cavity is formed by sandwiching a fuse-silica tube between a side-hole MF and a solid-core fiber. Using the holes in the MF as gas channels, the pressure in the FP cavity is controlled. The sensor was tested for operation above 1000 °C. Strain-insensitive temperature measurement was demonstrated at ambient temperature for a strain range up to 3600 $\mu\varepsilon$.**

***Index Terms*— Fiber-optic sensors, temperature measurement, microstructure fiber, Fabry–Pérot interferometer.**

I. Introduction

FIBER-OPTIC sensors have several advantages over other sensor technologies such as small size, light weight, immunity to electromagnetic interferences, remote sensing capability, and resistance to harsh environment. Various fiber-optic sensor technologies have been developed in the past decades for temperature measurement. Most of them are based on different types of interferometers, such as fiber Bragg gratings (FBGs) [1], [2], in-line Fabry–Pérot (FP) interferometers [3], [4], extrinsic FP interferometers [5]–[7], modal interferometers using SMF-multimode-SMF structures [8], or interferences of two polarizations [9]. The interference fringes of these interferometers are used to determine their characteristic optical path distance (OPD), nL, where n is the refractive index (RI) of the material that forms the interferometer and L is the characteristic length of the interferometer structure (e.g. for a FBG, L is the grating period; and for a FP cavity, L is the cavity length). Both n and L are temperature dependent (through the thermo-optic effect and the thermal expansion, respectively). However, temperature measurements are primarily achieved through the dominant thermo-optic effect due to the small coefficient of thermal expansion (CTE) of the fused silica material, about 5.5×10^{-7}/°C at room temperature. A drawback of these temperature sensors is the cross-sensitivity to the strain applied to the sensing elements, which are particularly problematic when the sensors are embedded into structures or experience high pressure variations. The strain-induced spectral changes are indistinguishable from temperature-induced ones and, consequently, cause temperature measurement errors. For example, a FBG typically has a temperature sensitivity of ~10 pm/°C and a strain sensitivity of ~1 pm/$\mu\epsilon$ [1], [2]. In addition, when the sensors are used for high temperature applications, the relaxation of the residual stresses induced during the sensor fabrication and the potential structural changes of the glass materials, such as devitrification, may change the cavity length as well and cause measurement errors. Complicated annealing process is required to increase the sensor stability and accuracy [4]. These sensors also suffer from their nonlinear response. Because the thermo-optic coefficient of the fused silica material used to form the FP cavity is a complex function of temperature, especially at high temperatures [10], the sensor responds nonlinearly to temperature. Another drawback for many of the sensors is the requirement for calibration. Because the sensor response may be dependent on the unique structural parameters of individual sensor, each sensor needs to be calibrated before it can be used for temperature measurement.

In this Letter, we report a fiber-optic temperature sensor with significantly reduced strain cross-sensitivity, linear response, enhanced temperature capability, small size, calibration-free operation, and capability for absolute measurement. The sensor consists of an in-line FP cavity formed by a fused-silica tube sandwiched between a solid SMF and a microstructure fiber (MF) with holes in the cladding. The operation is based on the dependence of the RI of a gas (air in this case) on both temperature and pressure. Using the holes in the MF as gas channels, the FP cavity is pressurized with gas of variable pressure [11]. The spectral shift of the FP interference fringes is recorded as the pressure is increased. The temperature is deduced from the optical wavelength and the slope of the spectral shift vs. pressure curve, which, as shown later, is largely independent on the cavity length, L. As a result, the temperature measurement is insensitive to strain or other structural changes to the FP cavity. The sensor, which is tested to operate from room temperature to above 1000 °C, has a diameter of only 125 μm and a sensing region of only ~60 μm.

Manuscript received January 22, 2014; accepted January 27, 2014. Date of publication February 11, 2014; date of current version March 20, 2014. This work was supported in part by the Office of Naval Research under Grants N000141110705 and N000141110262, and in part by the National Science Foundation under Grant EPS-1004094.

Y. Lu and M. Han are with the Department of Electrical Engineering, University of Nebraska-Lincoln, Lincoln, NE 68588 USA (e-mail: yujielu1219@gmail.com; mhan3@unl.edu).

J. Tian was with the Department of Electrical Engineering, University of Nebraska-Lincoln, Lincoln, NE 68588 USA. He is with the College of Electronic and Information Engineering, Shenzhen Graduate School, Harbin Institute of Technology, Shenzhen 518055, China (e-mail: jiajuntian@gmail.com).

Color versions of one or more of the figures in this letter are available online at http://ieeexplore.ieee.org.

Digital Object Identifier 10.1109/LPT.2014.2304297

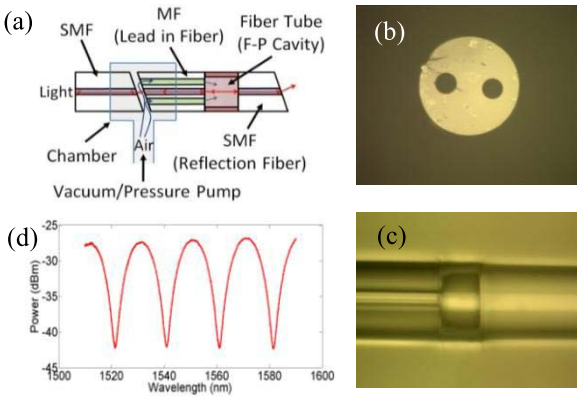

Fig. 1. (a) Schematic of sensor structure; (b) and (c) microscope pictures of the MF endface and the FP cavity; (d) reflection spectrum of the sensor at ambient temperature and pressure.

II. Operational Principle

The structure of the sensor, schematically shown in Fig. 1(a), consists of a lead-in MF, a fuse-silica tube, and a reflection SMF. The MF has a diameter of 125 μm. In its cladding, there are two holes with similar diameter of $\sim$26 μm running along the fiber length, as shown in Fig. 1(b). The MF and the SMF are cleaved and spliced to both ends of the tube using a fiber splicer to form an enclosed FP cavity. The cleaved ends of the fibers also serve as the reflectors of the FP cavity. The other end of the MF is connected to another SMF to transmit the reflected optical signal into the detection system. Meanwhile, the holes of the MF are used as gas channels to pressurize the FP cavity from inside. Both fibers in this connection are cleaved with an angle of $\sim$8° to avoid the undesirable reflections that may interfere with the signals from the FP cavity. They are placed close to each other and sealed in a 3-way pipeline connector that is connected to a vacuum/pressure pump. Fig. 1(c) is a microscope picture of the sensing region of fabricated sensor and Fig. 1(d) shows the interference spectrum of the reflected light from the sensor measured by a fiber sensor interrogator. From the spectrum, the cavity length is estimated to be $\sim$60 μm. Therefore, the overall diameter of the sensor is only $\sim$125 μm and the length of the sensing region is only $\sim$60 μm.

The wavelength corresponding to a constant phase on the fringe (e.g. a fringe valley or peak) is given by

$$2nL = m\lambda, \tag{1}$$

where m is a constant and λ is the wavelength of constant phase. In this case, n and L are, respectively, the RI of air and the FP cavity length. Due to the non-ideality of air, the RI of air is a complicated function of its temperature (T), pressure (p), and composition [12]. However, to a good degree of accuracy, the difference between the air RI and the vacuum RI is proportional to p/T (T in the unit of Kelvin) [13], or

$$n - 1 = \gamma\, p/T, \tag{2}$$

where γ is a constant whose value is determined by the gas type. Equations (1) and (2) yields

$$\lambda = \frac{2L}{m}\left(\frac{\gamma}{T}p + 1\right), \tag{3}$$

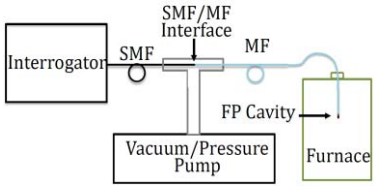

Fig. 2. Schematic of the experimental set up.

From (3), the slope of the λ vs. p curve, k, is dependent on the temperature. Assuming that the strain is constant when p is varied and ignoring the small dependence of L on p,

$$k \triangleq \frac{\partial\lambda}{\partial p} = \frac{2\gamma L}{mT} \tag{4}$$

Note that for gases, $n \approx 1$ (e.g. $n - 1 \approx 3 \times 10^{-4}$ for air at standard temperature and pressure) and, from (1), $L/m \approx \lambda/2$. Then (4) leads to

$$T = \gamma\,\lambda/k. \tag{5}$$

Equation (5) shows that the absolute gas temperature can be deduced from λ/k, which is obtained from the recorded reflection spectra, with a coefficient, γ, which is determined by the optical property of the gas. In addition to absolute temperature measurement, the sensor does not require calibration because the parameter, γ, is independent on the structure and the properties of the solid material forming the sensor.

III. Experiment And Discussion

The sensor shown in Fig. 1(c) was tested using a set up shown in Fig. 2. A vacuum/pressure pump was used to change the air pressures inside the FP cavity. A sensor interrogator was used to record the reflection spectrum of the sensor. The temperature was increased from the ambient temperature in the room to 1025 °C with a step of 25 °C using a furnace. At each step, the absolute pressure inside the sensor FP cavity was changed from 1 psi (partial vacuum), to ambient pressure, and to 1514 psi, with a step size of $\sim$60 psi between ambient pressure to 1514 psi. The length of the lead-in MF was $\sim$0.5 m and we found that it only took a few seconds for the reflection spectra to stabilize, indicating a balanced pressure in the cavity.

Fig. 3(a) and (b) show, respectively, the reflection fringes at different pressure levels at ambient temperature ($\sim$20 °C) and at 200 °C. For clarity, only the fringe valleys corresponding to the one around 1521.5 nm at 0 psi were shown. It is seen that, as pressure increased, the fringe shifted toward longer wavelength and the spectral shift was more sensitive to pressure changes at lower temperatures. For example, the fringe valley shifted toward the longer wavelength by 41.8 nm when the pressure increased from 0 to 1500 psi (gauge pressure) at 20 °C, corresponding to an increase of 0.027 in the air RI; while the fringe valley shifted only by 25.6 nm for the same pressure change at 200 °C, corresponding to an RI increase of 0.017.

Fig. 4 shows experimental results for the wavelength position, λ, of the same fringe valley as shown in Fig. 3 as a function of the pressure inside the FP cavity, p, at different temperatures and their least-square-error linear fittings. For clarity, the results are shown separately for two different

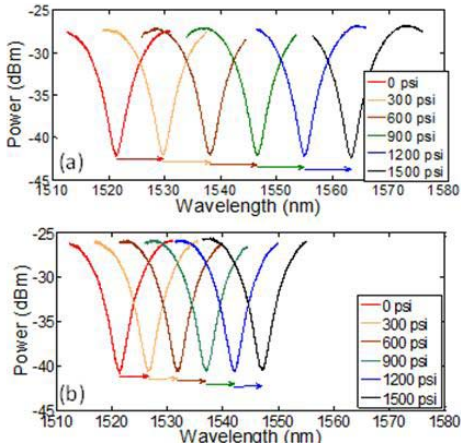

Fig. 3. Reflection spectra at different gauge pressure levels for two different temperatures: (a) ambient temperature (20 °C) and (b) 200 °C.

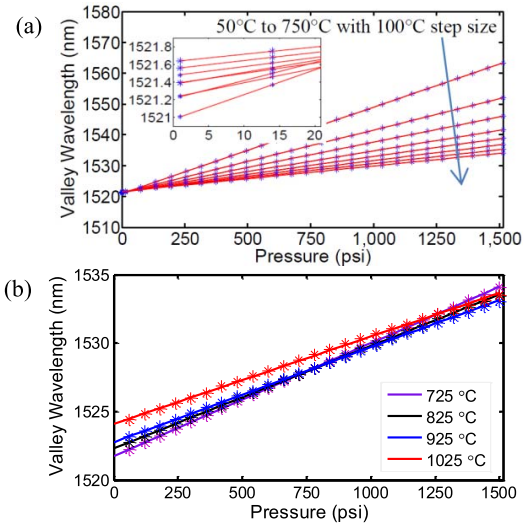

Fig. 4. Valley wavelength vs. pressure for temperature range of (a) 50 to 750 °C and (b) 725 to 1025 °C.

temperature ranges: Fig. 4(a) and (b) are, respectively, the results obtained when the temperature was increased from 50 to 750 °C and from 725 to 1025 °C. In agreement with (3), the experimentally-obtained λ vs. p curves for all temperatures show excellent linearity with the correlation coefficients, R, of the linear fitting lines very close to 1 (with $1-R$ ranging from 5.1×10^{-10} to 4.8×10^{-7}). From the inset to Fig. 4(a), it is seen that, when the gas pressure is low, the valley wavelength is largely insensitive to temperature. For example, a temperature change from 50 to 750 °C only leads to a variation of ~0.4 nm in the valley wavelength at ambient pressure (~14 psi) which is expected from the extremely low CTE of the fused-silica material. Interestingly, significant changes in the wavelength positions of the fringe valley at 0 psi were observed when the temperature was increased from 725 to 1025 °C, as shown in Fig. 4(b). Specifically, it was observed that the valley wavelength shifted nonlinearly with respect to the temperature toward the longer wavelength by ~2.5 nm for this temperature range, indicating a 0.16% increasing in the FP cavity length (equivalent to a strain of 1600 $\mu\varepsilon$). We believe that such a change, which cannot be accounted for by the thermal

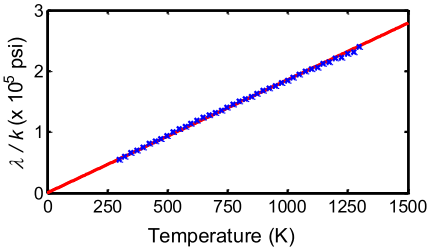

Fig. 5. Calculated λ/k vs. temperature and the line fitting using Eq. (5).

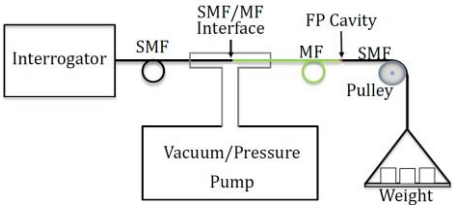

Fig. 6. Experimental set up for temperature measurement when the sensor is strained.

expansion of the material, is resulted from the relaxation of the residual stress that was introduced by the splicing process during the sensor fabrication. It is seen that, despite the thermally-induced cavity length changes, the fringe valley wavelength maintained a good linear relationship with the applied pressure in the FP cavity.

To validate the proposed temperature measurement method using (5), we calculated λ/k from the measured λ vs. p curve at each temperature (T), in which the slope of the linear fitting line shown in Fig. 4 was used for k and the average of the wavelength positions of the fringe valley for the pressure range from 0 to 1500 psi was used for λ. Fig. 5 shows the obtained λ/k vs T data points and the linear fitting line using (5). From the fitting line, $\gamma = 0.00538$ K/psi is obtained for air. It is worth noting that the results for the temperature range from 725 °C (998 K) to 1025 °C (1298 K), whose cavity length shows thermally-induced nonlinear changes, do not deviate from the linear fitting curve, which is an indication that the proposed temperature measurement method is immune to FP cavity length changes.

To further validate that the temperature sensor is insensitive to cavity length variations, we fabricated a new sensor with a much longer SMF pigtail fiber that allowed us to conveniently apply train to the sensing element. Using a setup schematically shown in Fig. 6, we performed measurements when different strains were applied on the sensor at an approximately constant ambiet temperature. In this experiment, the FP cavity was streched by applying different weight on the pigtail fiber through a pulley system and the strain ($\varepsilon = \Delta L/L$) was calculated from the wavelength shift of the fringe valley. The maximum strain applied on the sensor is estimated to be ~3600 $\mu\varepsilon$.

Fig. 7(a) shows the curves and their linear fitting lines for the measured wavelength position of a fringe valley as a function of pressure in the FP cavity when the sensor was applied to different strains. The curves again show excellent linearity with $1-R$ ranging between 2.1×10^{-8} and 2.4×10^{-8} over the whole strain range. For each of the curves, the value of λ/k was calculated following the same method used to obtain

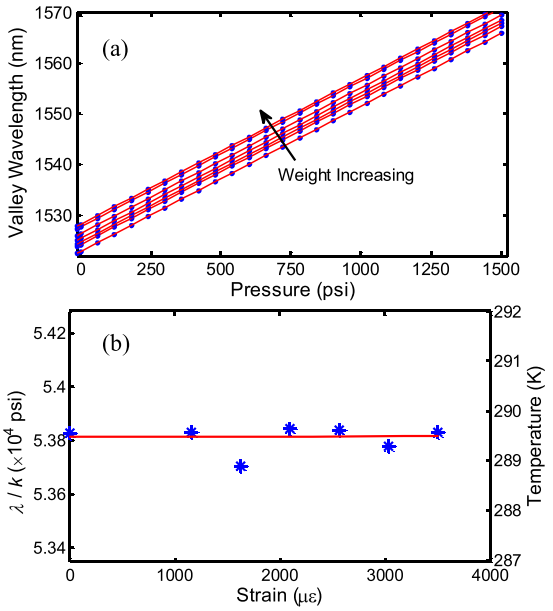

Fig. 7. (a) Valley wavelength vs. pressure when different strains were applied to the sensor. (b) Calculated λ/k and temperature vs. strain applied to the sensor and its linear fitting.

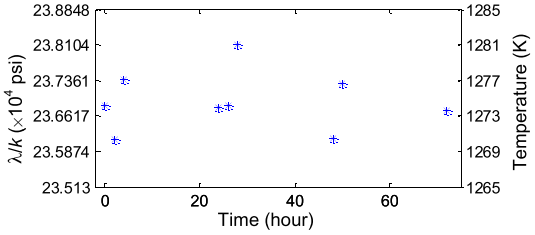

Fig. 8. Sensor high-temperature stability test: calculated λ/k and temperature from different measurements when the furnace temperature was set to 1000 °C (1273 K).

Fig. 5. Then using the coefficient $\gamma = 0.00538$ K/psi for air obtained from Fig. 5, the temperature was calculated. The results for the calculated λ/k and measured temperature as a function of the applied strain and the linear fitting line are shown in Fig. 7(b). It is seen that the peak-to-peak fluctuations for the measured temperature is only 0.76 K (0.76 °C) for the strain range up to 3600 $\mu\varepsilon$. Note that the fluctuations also include the random ambient temperature variations. On the contrary, if not compensated for, such a strain level can cause enormous temperature errors for the conventional FP or FBG-based sensors. For example, a strain of 3600 $\mu\varepsilon$ is equivalent to a temperature variation of ~360 °C for a FBG sensor. Therefore, it is validated that the demonstrated temperature measurement method is insensitive to strain.

Finally we tested the sensor stability for long-term operation at high temperatures. The sensor was placed in the furnace (Model: F47914, Thermo Scientific) set at 1000 °C (1273 K) for 3 days. The absolute temperature was measured 9 times during the process, as shown in Fig. 8. The average of the measured temperature is 1274.6 K (1001.6 °C). No systematic long-term temperature drift was observed. The standard deviation of the measured temperature is only 3.3 K (~ 0.26% of the absolute temperature) and the peak-to-peak variation is 10.6 °C (10.6 K). This test is limited by the accuracy (± 3 °C) and temperature uniformity (± 4.8 °C) of the furnace.

We note that the slope, k, can be obtained by recording only two spectra at two different pressure levels, which can significantly reduce the complexity of sensor operation and increase the measurement speed. In addition, the method has assumed that the strain is constant when the pressure is varied during each measurement, which is valid in many applications.

IV. Conclusion

We have proposed and demonstrated a novel high temperature fiber-optic FP interferometric sensor that is insensitive to FP cavity length variations and can perform calibration-free measurement of absolute temperature. The FP cavity is formed by splicing a side-hole MF and a solid SMF on a short fuse-silica tube. The sensor is operated by tuning the gas pressure inside the FP cavity through the holes in the MF and recording the wavelength position of a constant-phase point on the spectral fringes. Temperature measurement is achieved from the wavelength position of the point and the slope of the wavelength position vs. pressure curve. We theoretically and experimentally show that this unexplored temperature sensing mechanism is inherently insensitive to the variations of the FP cavity length and the absolute temperature can be obtained without the need for calibration. The sensor is tested for successful operation at temperature above 1000 °C. Long-term stability test at 1000 °C was also tested. The sensor is miniaturized with a diameter of ~125 μm and a length of ~60 μm in the sensing region.

References

[1] K. O. Hill and G. Meltz, "Fiber Bragg grating technology fundamentals and overview," *J. Lightw. Technol.*, vol. 15, no. 8, pp. 1263–1276, Aug. 1997.

[2] A. D. Kersey, *et al.*, "Fiber grating sensors," *J. Lightw. Technol.*, vol. 15, no. 8, pp. 1442-1463, Aug. 1997.

[3] H. Y. Choi, *et al.*, "Miniature fiber-optic high temperature sensor based on a hybrid structured fabry-perot interferometer," *Opt. Lett.*, vol. 33, no. 21, pp. 2455–2457, Nov. 2008.

[4] D. W. Duan, *et al.*, "In-line all-fibre fabry-perot interferometer high temperature sensor formed by large lateral offset splicing," *Electron. Lett.*, vol. 47, no. 6, pp. 401–402, Mar. 2011.

[5] Y. Z. Zhu, E. M. Lally, B. Dong, J. Gong, and A. Wang, "Sapphire-fiber-based white-light interferometric sensor for high-temperature measurements," *Opt. Lett.*, vol. 30, no. 7, pp. 711–713, Apr. 2005.

[6] J. J. Wang, *et al.*, "Fabrication of a miniaturized thin-film temperature sensor on a sapphire fiber tip," *IEEE Sensors J.*, vol. 11, no. 12, pp. 3406–3408, Dec. 2011.

[7] J. Ma, J. Ju, L. Jin, W. Jin, and D. Wang "Fiber-tip micro-cavity for temperature and transverse load sensing," *Opt. Express*, vol. 19, no. 13, pp. 12418–12426, Jun. 2011.

[8] S. M. Tripathi, A. Kumar, R. K. Varshney, Y. B. P. Kumar, E. Marin, and J.-P. Meunier, "Strain and temperature sensing characteristics of single-mode-multimode-single-mode structures," *J. Lightw. Technol.*, vol. 27, no. 13, pp. 2348–2356, Jul. 1, 2009.

[9] Y. B. Zhang, G. R. Pickrell, B. Qi, A. Safaai-Jazi, and A. Wang, "Single-crystal sapphire based optical polarimetric sensor for high temperature measurement," *Sensors*, vol. 6, no. 8, pp. 823–834, Aug. 2006.

[10] G. Adamovsky, *et al.*, "Peculiarities of thermo-optic coefficient under different temperature regimes in optical fibers containing fiber Bragg gratings," *Opt. Commun.*, vol. 285, no. 5, pp. 766–773, Mar. 2012.

[11] J. J. Tian, Q. Zhang, T. Fink, H. Li, W. Peng, and M. Han, "Tuning operating point of extrinsic Fabry-Perot interferometric fiber-optic sensors using microstructured fiber and gas pressure," *Opt. Lett.*, vol. 37, no. 22, pp. 4672–4674, Nov. 2012.

[12] P. E. Ciddor, "Refractive index of air: New equations for the visible and near infrared," *Appl. Opt.*, vol. 35, no. 9, pp. 1566–1573, Mar. 1996.

[13] P. R. N. Childs, *Practical Temperature Measurement*. Oxford, U.K: Butterworth-Heinemann, 2001, p. 290.